Extraction of Electrode Kinetic Parameters from Microdisc Voltammetric Data Measured under Transport Conditions Intermediate between Steady-State Convergent and Transient Linear Diffusion As Typically Applies to Room Temperature Ionic Liquids

Alexander S. Barnes,[†] Emma I. Rogers, Ian Streeter,[†] Leigh Aldous,[‡] Christopher Hardacre,[‡] and Richard G. Compton*,[†]

Department of Chemistry, Physical and Theoretical Chemistry Laboratory, Oxford University, South Parks Road, Oxford OX1 3QZ, United Kingdom, and School of Chemistry and Chemical Engineering/QUILL, Queen's University Belfast, Belfast, Northern Ireland BT9 5AG, United Kingdom

Received: December 19, 2007; Revised Manuscript Received: March 14, 2008

The extraction of electrode kinetic parameters for electrochemical couples in room-temperature ionic liquids (RTILs) is currently an area of considerable interest. Electrochemists typically measure electrode kinetics in the limits of either transient planar or steady-state convergent diffusion for which the voltammetic response is well understood. In this paper we develop a general method allowing the extraction of this kinetic data in the region where the diffusion is intermediate between the planar and convergent limits, such as is often encountered in RTILs using microelectrode voltammetry. A general working surface is derived, allowing the inference of Butler−Volmer standard electrochemical rate constants for the peak-to-peak potential separation in a cyclic voltammogram as a function of voltage scan rate. The method is applied to the case of the ferrocene/ferrocenium couple in $[C_2mim][N(Tf)_2]$ and $[C_4mim][N(Tf)_2]$.

1. Introduction

The measurement of electrochemical rate constants lies at the heart of interfacial studies and is usually approached by voltammetric methods in which current is measured as a function of an applied voltage.

The two limiting types of investigation are familiar to all electrochemists. The first corresponds to the use of microelectrodes under essentially steady-state, convergent diffusion conditions, where a sigmoidal curve is obtained and typically analyzed by the procedure of Mirkin and Bard.[1] This gives values for the electrochemical rate constant and transfer coefficient assuming Butler−Volmer kinetics.[2] The technique utilizes the potentials corresponding to a quarter and three-quarters of the limiting current and appropriate tables of data.

The second limit is that of conventional cyclic voltammetry under linear diffusion conditions.[2] Here, a triangular voltage scan is applied, and a cyclic voltammogram recorded. In this case the variation of peak-to-peak separation, ΔE_{pp}, as a function of the voltage scan rate, reveals the sought-after electrode kinetic data. This limit is typically encountered in conventional solvents when using macroelectrodes. Alternatively, Amatore has used megavolt per second cyclic voltammetry at microdisc electrodes in order to extract electrode kinetic data and, in doing so, reached the linear diffusion limit in conventional electrochemical solvents such as acetonitrile.[3,4]

Aoki[5] showed that the diffusional behavior depends on a single parameter, σ, the dimensionless voltage scan rate defined in eq 1 and also in Table 1.

$$\sigma = \frac{F}{RT}\frac{r_d^2}{D_A}\nu \tag{1}$$

It was shown by numerical simulation that the transition from convergent to planar diffusion corresponds to the range $0.076 \leq \sigma^{1/2} \leq 150$ over which intermediate diffusional behavior is observed.

This intermediate behavior is often encountered in the case of voltammetry at microelectrodes in room-temperature ionic liquids (RTILs). Indeed some of the diffusion coefficients of differently charged but otherwise similar species can be significantly different so that both types of behavior can sometimes be seen in the same voltammogram, as reported for the $O_2/O_2^{\bullet-}$ couple in $[N_{6222}][N(Tf)_2]$.[6] Since the investigation of electron transfer kinetics in RTILs is currently of significant interest,[7–9] we present in this paper a general analysis of this intermediate kinetic region and apply our theory to the extraction of electrochemical rate constants for the ferrocene/ferrocenium couple in two RTILs.

2. Simulation Method

This section describes the modeling of the following simple heterogeneous process at a microdisc electrode:

$$A - e^- \rightleftharpoons B \tag{2}$$

Diffusion to the electrode surface is described by Fick's second law, expressed in cylindrical polar coordinates (z, r) for species A and B, respectively, in eqs 3 and 4.

$$\frac{\partial[A]}{\partial t} = D_A\left(\frac{\partial^2[A]}{\partial z^2} + \frac{\partial^2[A]}{\partial r^2} + \frac{1}{r}\frac{\partial[A]}{\partial r}\right) \tag{3}$$

$$\frac{\partial[B]}{\partial t} = D_B\left(\frac{\partial^2[B]}{\partial z^2} + \frac{\partial^2[B]}{\partial r^2} + \frac{1}{r}\frac{\partial[B]}{\partial r}\right) \tag{4}$$

For the purposes of the simulation, the model is normalized using dimensionless parameters, which are summarized in Table

* Corresponding author. Address: Physical and Theoretical Chemistry Laboratory, Oxford University, South Parks Road, Oxford, United Kingdom OX1 3QZ. Fax: +44 (0) 1865 275410. Tel: +44 (0) 1865 275413. E-mail: richard.compton@chem.ox.ac.uk.

[†] Oxford University.

[‡] Queen's University Belfast.

10.1021/jp711897b CCC: $40.75
Published on Web 05/29/2008

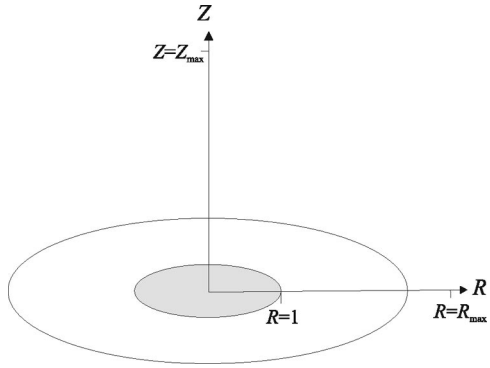

Figure 1. Diagram of the microdisc simulation space.

TABLE 1: Dimensionless Parameters Used for Numerical Simulation

parameter	expression
concentration of species A	$a = [A]/[A]_{bulk}$
concentration of species B	$b = [B]/[A]_{bulk}$
radial coordinate	$R = r/r_d$
normal coordinate	$Z = z/r_d$
time	$\tau = (D_A t)/r_d^2$
scan rate	$\sigma = (F/RT)[(\nu r_d^2)/D_A]$
potential	$\theta = (F/RT)(E - E_f)$
heterogeneous rate constant	$K_0 = (k_0 r_d)/D_A$

1. Space is described by the normalized (R,Z)-coordinate system shown in Figure 1, where $R = r/rd$ and $Z = z/rd$, species A and B are described by their normalized concentrations, a and b, and time, t, is normalized to the dimensionless τ. Equations 3 and 4 can therefore be expressed as eqs 5 and 6 by making use of these dimensionless parameters.

$$\frac{\partial a}{\partial \tau} = \left(\frac{\partial^2 a}{\partial Z^2} + \frac{\partial^2 a}{\partial R^2} + \frac{1}{R}\frac{\partial a}{\partial R}\right) \tag{5}$$

$$\frac{\partial b}{\partial \tau} = \frac{D_B}{D_A}\left(\frac{\partial^2 b}{\partial Z^2} + \frac{\partial^2 b}{\partial R^2} + \frac{1}{R}\frac{\partial b}{\partial R}\right) \tag{6}$$

To simulate a cyclic voltammogram, the dimensionless potential, θ, defined as $F/RT(E - E_f)$, is swept from an initial value, θ_i, to a more oxidizing potential, θ_f, and then back to the initial value. The value of θ is therefore calculated at any time on the forward sweep using eq 7 and on the reverse sweep using eq 8, where σ is the dimensionless scan rate as defined in Table 1, and the dimensionless time, τ, is defined as $(D_A t)/r_d^2$.

$$\theta = \theta_i + \sigma\tau \tag{7}$$

$$\theta = 2\theta_f - \theta_i - \sigma\tau \tag{8}$$

The concentration profiles for A and B are obtained by solving eqs 5 and 6 subject to the boundary conditions given in Table 2. The boundary condition at the electrode surface is derived from Butler−Volmer kinetics describing electron transfer.

$$\left(\frac{\partial a}{\partial z}\right) = K_0(e^{(1-\alpha)\theta}a_0 - e^{-\alpha\theta}b_0) \tag{9}$$

By inspection of the mass transport equations 5 and 6 and the boundary conditions given in Table 2, we can infer that the dimensionless peak-to-peak separation of the simulated voltammograms will depend only on K_0, σ, and the ratioD_B/D_A.

Equations 5 and 6 are discretized over a simulation grid and solved using the alternating direction implicit (ADI) method[10] coupled with the Thomas algorithm.[11] The simulation grid is constructed such that the mesh density is greatest around the

TABLE 2: Boundary Conditions for Eqs 5 and 6

boundary	condition for A	condition for B
$\tau = 0$, all r, z	$a = 1$	$b = 0$
$z = 0$, $r > r_d$	$(\partial a/\partial z) = 0$	$(\partial b/\partial z) = 0$
$z = 0$, $r \le r_d$	$(\partial a/\partial z) = K_0(e^{(1-\alpha)\theta}a_0 - e^{-\alpha\theta}b_0)$	$D_A(\partial a/\partial z) = -D_B(\partial b/\partial z)$
$z \ge 0$, $r = 0$	$\partial a/\partial r = 0$	$\partial b/\partial r = 0$
$z \to \infty$, $r \ge 0$	$a = 1$	$b = 0$
$z \ge 0$, $r \to \infty$	$a = 1$	$b = 0$

singularity at $R = 1$ and adjacent to the electrode surface at $Z = 0$. This is achieved by using a pair of parameters, h_0, defining the mesh spacing adjacent to the singularity and electrode surface, and γ, the factor by which each successive mesh spacing increases relative to h_0 as descibed by Gavaghan.[12] Having tested for convergence, the values used in this paper are $\gamma = 1.175$ and $h_0 = 8 \times 10^{-5}$.

The dimensionless diffusional flux is calculated from the concentration profile of species A using second-order finite difference methods and eq 10.

$$j = \int_0^1 \left(\frac{\partial a}{\partial Z}\right)_{z=0} R\mathrm{d}R \tag{10}$$

The measured current, I, is related to the dimensionless flux by eq 11.

$$I = 2\pi nFD_a r_d [A]_{bulk} j \tag{11}$$

All programs used to perform these simulations were implemented in C++ and run on a desktop PC with a 3.4 GHz Pentium processor and 2GB of RAM.

3. Simulated Results

Here we present and explain the results of an investigation into the variation of peak-to-peak separation, $\Delta\theta_{pp}$, for a wide range of scan rates and heterogeneous rate constants. We shall discuss the various limiting behaviors of $\Delta\theta_{pp}$ and, where possible, paramaterize the observed trends. The simulations in this section were all carried out with $D_A = D_B$ and transfer coefficient $\alpha = 1/2$.

At high scan rates, the disk radius, r_d, is much larger than the thickness of the diffusion layer above the electrode. Therefore, diffusion is described by a planar model, and the voltammetry, which is shown in Figure 2b, closely resembles that at a macroelectrode. This macroelectrode-type behavior has been previously characterized by Nicholson and Shain.[13] They have shown that, within this planar diffusional model, in the irreversible limit (slow electrode kinetics), the peak-to-peak separation displays a linear dependence, and the peak positions are described by eq 12.

$$E_p = E^0 + \frac{RT}{\alpha F}\left(0.780 + \ln\left(\frac{\alpha F}{RT}\frac{\nu D}{k_0^2}\right)^{1/2}\right) \tag{12}$$

For the case of $D_A = D_B$ the forward and reverse peak potentials are symmetric about E^0, therefore, provided $\alpha = \beta = 0.5$, we can use eq 12 to derive eq 13, which describes the peak-to-peak separation in the limit of planar diffusion and slow electrode kinetics.

$$\Delta E_{pp} = \frac{2RT}{\alpha F}\left(0.780 + \ln\left(\frac{\alpha F}{RT}\frac{\nu D}{k_0^2}\right)^{1/2}\right) \tag{13}$$

In the reversible limit (fast electrode kinetics) under planar diffusion conditions, the peak-to-peak separation tends toward

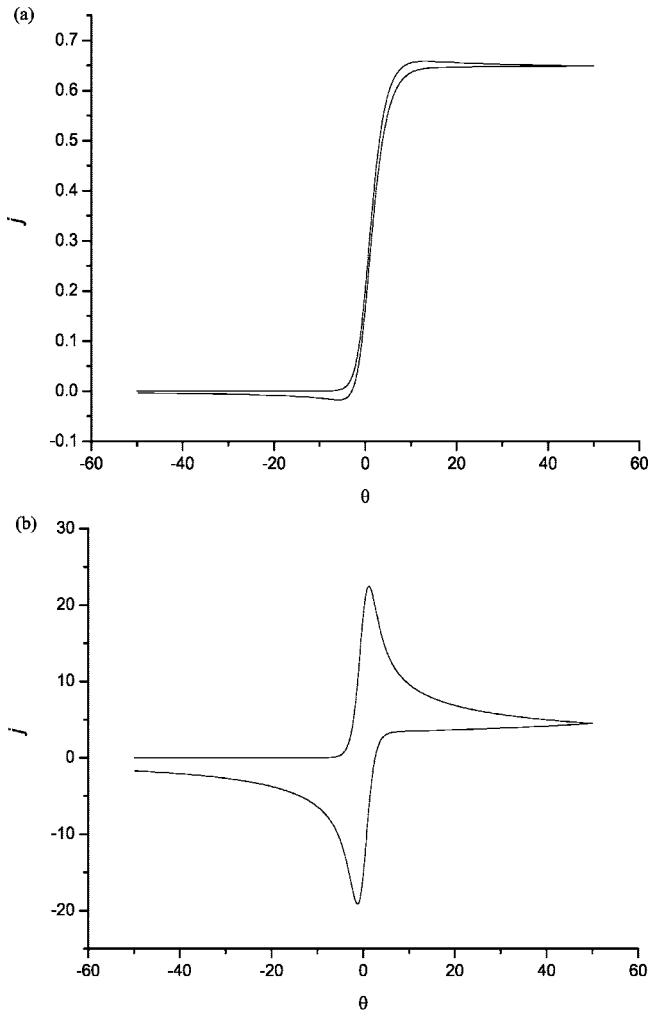

Figure 2. Simulated voltammetry at a microdisc electrode: (a) $\sigma = 10^{-1}$, $K_0 = 1$ and (b) $\sigma = 10^4$, $K_0 = 10^3$.

59 mV with little scan rate dependence, indicative of a system displaying Nernstian type behavior.

Conversely, at low scan rates, the diffusion layer thickness is large relative to r_d; therefore diffusion is described by a convergent model. The resultant voltammetry shows near-steady-state behavior illustrated in Figure 2a with a dimensionless flux, j, tending toward $2/\pi$ as predicted by Saito.[14]

We shall now consider the variation of the peak-to-peak separation with scan rate in the limit of irreversible electrode kinetics at both fast and slow scan rates. In this irreversible limit at slow scan rates, the peak to peak separation shows an initial decrease with increasing scan rate. This is due to the transition from a convergent diffusional model to one in which planar diffusion begins to dominate; the range of σ values over which this transition occurs has been quantified in Section 1. The decrease in peak separation can be inferred from Figure 3b since we have noted that the forward and reverse peaks are symmetric about E^0. At high scan rates, the diffusion is described by a planar diffusional model, and the peak-to-peak separation now increases with increasing scan rate. This trend can be inferred from Figure 3a. This increase in peak-to-peak separation is described by eq 12 and occurs because the electron transfer is apparently more irreversible on these faster experimental timescales.

The measured peak-to-peak separations for the full range of K_0 and σ values are shown as a working surface in Figure 4. In section 2 we asserted that the shape of the voltammogram

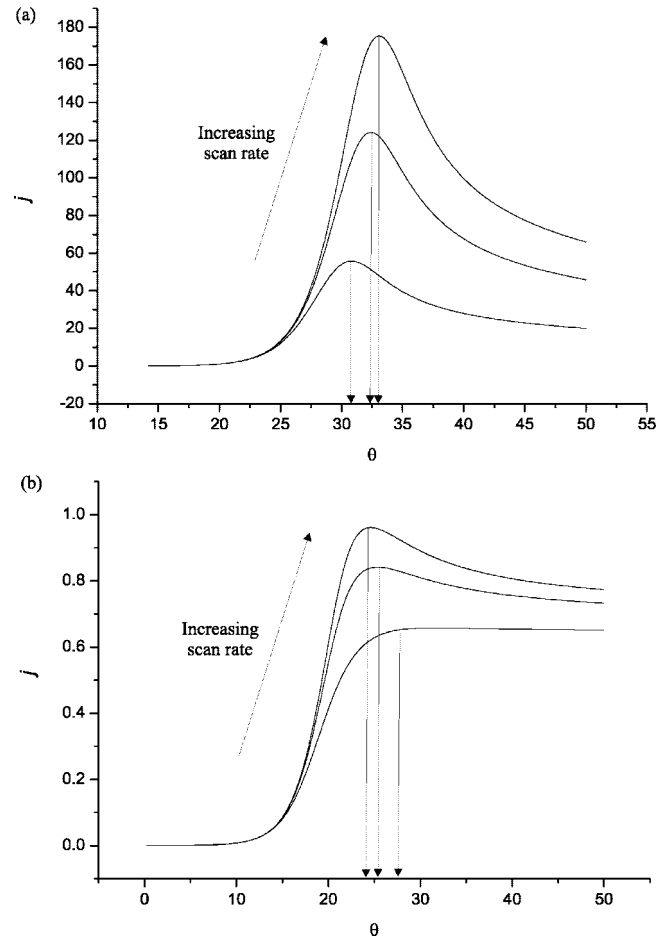

Figure 3. Plots illustrating the variation in forward peak position and dimensionless flux for $K_0 = 10^{-4}$: (a) $\sigma = 10^5$, 5×10^5, 10^6 and (b) $\sigma = 10^{-1}$, 5, 10.

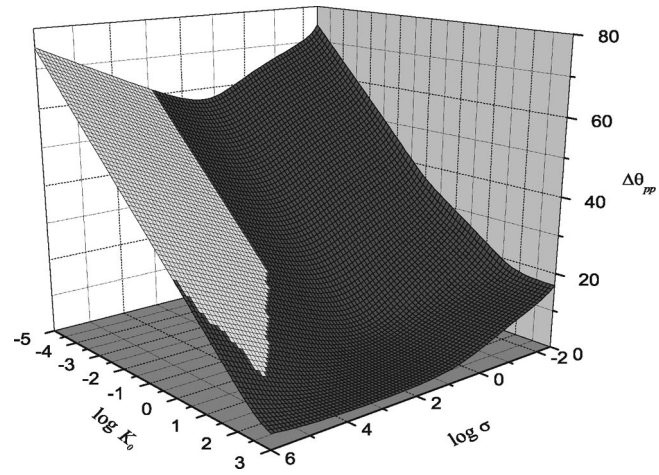

Figure 4. Plot of $\Delta\theta_{pp}$ as a function of σ and K_0.

depends only on K_0, σ, and the ratio D_B/D_A; since we have defined $D_A = D_B$, we can be sure that the peak-to-peak separation will depend only on K_0 and σ. This is the basis for plotting the working surface as shown in Figure 4. The shaded region on the surface defines the range of K_0 and σ values for which the peak-to-peak separations are predicted by eq 14 within experimental error. This corresponds to irreversible electron transfer under planar diffusion conditions; consequently, the voltammetric response is well described by analytical equations and macroelectrode-type behavior is observed. The bounds of this region were determined by generating an equivalent surface

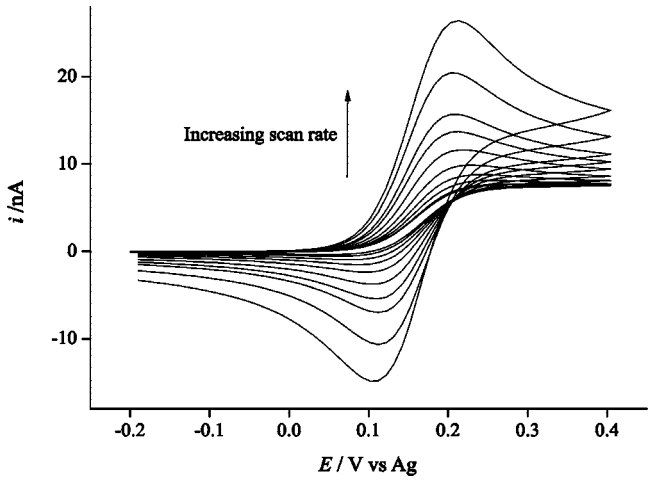

Figure 5. Cyclic voltammograms showing the reduction of saturated Ferrocene in $[C_2mim][N(Tf)_2]$ on a 10 m diameter Pt electrode at $\nu = 10$ mV s^{-1} to $\nu = 4000$ mV s^{-1}.

using eq 14 and calculating the points at which the peak-to-peak separations agree to within 0.2 θ units, equivalent to 5 mV at 298 K. Equation 14 has been presented in a way that allows the prediction of peak-to-peak separations for the case where $\alpha \neq \beta$ and $D_A \neq D_B$ for irreversible electron transfer under conditions of planar diffusion.

$$\Delta\theta_{pp} = \frac{1}{\alpha\beta}\left(0.780 + \ln\left(\frac{\alpha\sigma}{K_0^{\,2}}\right)^{\frac{1}{2}}\right) + \frac{1}{\beta}\ln\left(\frac{\beta}{\alpha}\frac{D_B}{D_A}\right)^{\frac{1}{2}} \quad (14)$$

Having investigated the dependence of $\Delta\theta_{pp}$ on K_0 and σ, we will now make use of this dependence as a diagnostic tool for fitting experimental data.

4. Experimental Section

4.1. Chemical Reagents. Ferrocene ($Fe(C_5H_5)_2$, Aldrich, 98%), acetonitrile (MeCN, Fischer Scientific, dried and distilled, 99%) and tetra-*n*-butylammonium perchlorate (TBAP, Fluka, Puriss electrochemical grade, 99%) were used as received without further purification. 1-Ethyl-3-methylimidazolium bis-(trifluoromethylsulfonyl)imide, $[C_2mim][N(Tf)_2]$ and 1-butyl-3-methylimidazolium bis(trifluoro-methylsulfonyl)imide, $[C_4mim][N(Tf)_2]$ were prepared by standard literature procedures.[15,16]

4.2. Instruments. All electrochemical experiments were performed using a computer-controlled μ-Autolab potentiostat (Eco-Chemie, Netherlands). A conventional two-electrode arrangement was used to study the voltammetry of Fc, consisting of a 10 μm diameter platinum working electrode and a 0.5 mm diameter silver wire quasi-reference electrode. A small section of disposable pipet tip was used to form a cavity on the microelectrode surface, into which microlitre quantities of the RTIL solvent is added (typically 20 μL). The electrodes were housed in a T-cell (reported previously),[17,18] which is specially designed to allow samples to be studied under a controlled atmosphere. The liquid was purged under vacuum prior to, and during, experimental analysis. All experiments were undertaken in a heated Faraday cage (298 ± 1 K), which also served to minimize noise.

Saturated solutions of Fc were made up directly in 60 μL of ionic liquid and stirred for ca. 12 h. Twenty microliters of this solution was then placed in the T-cell, and electrochemical analysis was undertaken. The microdisk working electrode was polished using 1.0 μm and 0.3 μm water−alumina (Kemet Ltd., U.K.) slurry, respectively, on soft lapping pads (Buehler, Illinois), prior to each experiment. The electrode was calibrated by analyzing the steady-state voltammetry of a 2 mM solution of Fc in acetonitrile containing 0.1 M TBAP, to give the electrode diameter, adopting a value of D of ferrocene in MeCN of 2.3×10^{-9} m^2 s^{-1}.[19]

4.3. Double Potential Step Chronoamperometric Experiments. Double potential step chronoamperometric transients were achieved using a sample time of 0.01 s. The solution was pretreated by holding potential for 20 s at a point of zero faradaic current, after which the potential was stepped to a position after the oxidative peak of Fc, and the current was measured for 5 s. The potential was then stepped back to a point of zero current, and the current response measured for a further 5 s. Diffusion coefficients and solubility data for Fc were extracted from these transients by fitting the first potential step, using the nonlinear curve fitting function in the software package Origin 7.0 (Microcal Software, Inc.) The equations below were proposed by Shoup and Szabo[20] for the time-dependent current response at microdisk electrodes. The equations used in this approximation are sufficient to describe the current response to within an accuracy of 0.6%.

$$I = -4nFDcr_d f(\tau) \quad (15)$$

$$f(\tau) = 0.7854 + 0.8863\tau^{-1/2} + 0.2146\exp(-0.7823\tau^{-1/2}) \quad (16)$$

$$\tau = \frac{4Dt}{r_d^2} \quad (17)$$

where n is the number of electrons transferred, F is the Faraday constant, D is the diffusion coefficient, c is the initial concentration of parent species, r_d is the radius of the disk electrode, and t is the time. The value for the radius (previously calibrated) was fixed, and 100 iterations were performed by the software to give a value for the diffusion coefficient and the product of the number of electrons multiplied by concentration after optimization of the experimental data. A computer simulation program, described by Klymenko et al.[21] was employed to model the second potential step, allowing diffusion coefficient data for Fc^+ to be extracted. Values of D and nc obtained previously from Shoup and Szabo[20] analysis of the experimental data were input into the simulation software and values of D for this reverse step were varied until the best fit between theoretical and experimental data was achieved.

5. Results and Discussion

5.1. Cyclic Voltammetry for the Electrochemical Oxidation of Ferrocene in $[C_2mim][N(Tf)_2]$ and $[C_4mim][N(Tf)_2]$. The oxidation of ferrocene was studied in two RTILs on a 10 μm diameter platinum electrode at scan rates from 10 to 4000 mV s^{-1}. The voltammetry of saturated ferrocene (ca. 66.84 mM determined from potential step chronoamperometry) is shown in Figure 5. Ferrocene is oxidized to Fc^+ by one electron at a potential of +0.21 V versus Ag (for $[C_2mim][N(Tf)_2]$) and reduced at a potential of +0.11 V versus Ag. Equation 18 shows the electrode process.

$$[Fe(C_5H_5)_2] \rightleftharpoons [Fe(C_5H_5)_2]^+ + e^- \quad (18)$$

In order to calculate the diffusion coefficient of Fc and its oxidized species, Fc^+, double potential step chronoamperometry was performed. For the first step the potential was stepped from −0.10 V to +0.40 V, corresponding to the oxidation of Fc to Fc^+. The potential was then stepped back from +0.40 V to −0.10 V, corresponding to the reduction of Fc^+ to Fc. The

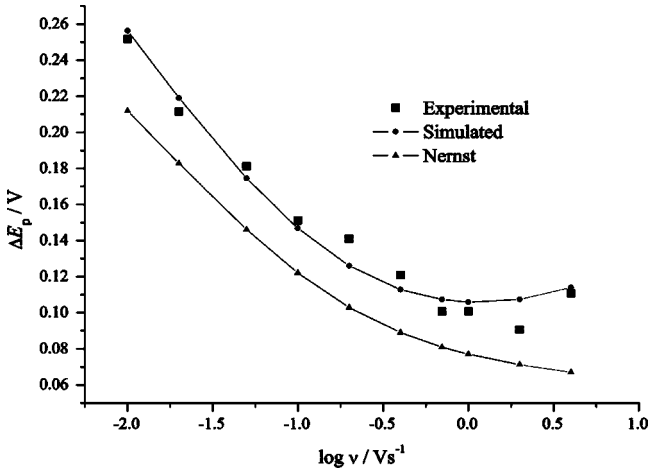

Figure 6. A plot illustrating the peak separations for the experimental, simulated, and reversible limit voltammetry of Fc in $[C_2mim][N(Tf)_2]$ over the entire range of scan rates. The simulation was carried out using $D_A = 4.60 \times 10^{-11}$ m^2 s^{-1}, $D_B = 3.3 \times 10^{-11}$ m^2 s^{-1} and $k_0 = 7.5 \times 10^{-3}$ cm s^{-1}.

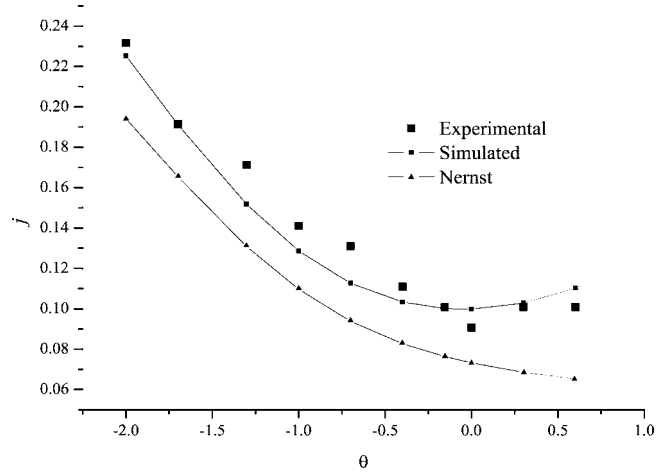

Figure 7. A plot illustrating the peak separations for the experimental, simulated, and reversible limit voltammetry of Fc in $[C_4mim][N(Tf)_2]$ over the entire range of scan rates. The simulation was carried out using $D_A = 2.82 \times 10^{-11}$ m^2 s^{-1}, $D_B = 2.0 \times 10^{-11}$ m^2 s^{-1} and $k_0 = 6.0 \times 10^{-3}$ cm s^{-1}.

diffusion coefficient, D, and solubility, c, of neutral Fc was determined from Shoup and Szabo[20] analysis of the experimental data for the first potential step. D_{Fc} and c values of 4.60×10^{-11} m^2 s^{-1} $\pm$ 0.05 and 66.84 mM $\pm$ 1.2 in $[C_2mim][N(Tf)_2]$ and 2.82×10^{-11} m^2 s^{-1} $\pm$ 0.05 and 61.09 mM $\pm$ 0.5 in $[C_4mim][N(Tf)_2]$ were achieved.

The peak-to-peak separation, ΔE_{pp}, decreases with increasing scan rate in the low scan rate limit. This is due to the transition from convergent to more planar diffusion as discussed fully in section 3 and illustrated in Figure 4. We can conclude that the observed voltammetry is an intermediate of micro/macroelectrode behavior.

By using peak-to-peak separation as the criterion for a successful fit, least-squares methods were employed to determine the value of k_0 providing the best agreement with experimental data across the entire range of scan rates. All parameters used in the simulations except the heterogeneous rate constant, k_0, were those determined experimentally. The values of the heterogeneous rate constant giving the best fit are $k_0 = 7.5 \times 10^{-3}$ cm s^{-1} in $[C_2mim][N(Tf)_2]$ and $k_0 = 6.0 \times 10^{-3}$ cm s^{-1} in $[C_4mim][N(Tf)_2]$. Figures 6 and 7 compare the peak-to-peak separations obtained from simulating the voltammetry using these best fit k_0 values and those obtained experimentally in $[C_2mim][N(Tf)_2]$ and $[C_4mim][N(Tf)_2]$, respectively. The values of k_0 obtained in these RTILs are slower than those obtained from experiments conducted in conventional aprotic solvents. This is not unexpected for an electron transfer occurring within a solvent composed entirely of charged species as opposed to conventional dipolar solvents. The plots in Figures 6 and 7 also show the Nernstian (fast electrode kinetics limit) values and demonstrate that the voltammetry is not well described by a fast reversible model.

That said, it is interesting to compare the inferred k_0 with other studies of the ferrocene/ferrocenium couple in RTILs. First we note that Bond et al.[7] report a value of $k_0 = 2.5 \times 10^{-3}$ cm s^{-1} in $[C_4mim][PF_6]$. In contrast, Hapiot[8] and some of the current authors[22] suggest that it is close to 0.2 cm s^{-1}. In the latter case, steady-state microelectrode measurements under a fast convection regime were used to remove complications due to capacitative charging. This suggests, as stressed by Bond,[7] Doherty,[9] and Hapiot,[8] that ohmic distortions may play a significant role in the transient cyclic voltammetry experiments.

Estimates of the likely "*iR*" drop[23] suggest that this is unlikely to be dominant in the experiments reported above, because of the rather small currents drawn. However, such estimates depend on RTIL conductivity data, for which detailed frequency effects have not been fully explored. Accordingly, the pertinent values for the slow scan cyclic voltammetry experiments reported above are likely unknown. Therefore it is best to regard the k_0 values reported in this paper as "apparent" values, following the good advice of Doherty.[9]

Finally we note that the theory reported above precisely defines the upper limit of heterogeneous rate constants that can be measured in RTILs using cyclic voltammetry.

6. Conclusions

In this paper we have developed a generic theory for the extraction of electrode kinetic parameters from microdisc voltammetry in the region of intermediate diffusional behavior. We have successfully applied this theory to the case of the ferrocene/ferrocenium couple in two ionic liquids and shown that the heterogeneous rate constants for these cases are probably slower than those of conventional aprotic solvents for the case of the ferrocene/ferrocenium couple. We envisage that this generic method will be useful for extracting kinetic parameters for other electrochemical couples in RTILs.

References and Notes

(1) Mirkin, M.; Bard, A. J. J. *Electroanal. Chem.* **1992**, *64*, 2293–2302.
(2) Compton, R. G.; Banks, C. E. *Understanding Voltammetry*; World Scientific: Singapore, 2006.
(3) Amatore, C.; Maisonhaute, E.; Simoneau, G. *Electrochem. Commun.* **2000**, *2*, 81–84.
(4) Amatore, C.; Maisonhaute, E.; Simoneau, G. J. *Electroanal. Chem.* **2000**, *486*, 141–155.
(5) Aoki, K.; Akimoto, K.; Tokuda, K.; Matsuda, H. J. *Electroanal. Chem.* **1984**, *171*, 219–330.
(6) Buzzeo, M. C.; Klymenko, O. V.; Wadhawan, J. D.; Hardacre, C.; Seddon, K. R.; Compton, R. G. *J. Phys. Chem. A* **2003**, *107*, 8872–8878.
(7) Zhang, J.; Bond, A. M. *Anal. Chem.* **2003**, *75*, 2694–2702.
(8) Lagrost, C.; Carrié, D.; Vaultier, M.; Hapiot, P. J. *Phys. Chem. A* **2003**, *107*, 745–752.
(9) Doherty, A. P.; Brooks, C. A. *Electrochim. Acta* **2004**, *49*, 3821–3826.
(10) Peaceman, J. W.; Rachford, H. H. J. *Soc. Ind. Appl. Math.* **1955**, *3*, 28–41.

(11) Atkinson, K. E. *Elementary Numerical Analysis*; John Wiley and Sons: New York, 2004.
(12) Gavaghan, D. J. J. *Electroanal. Chem.* **1998**, *456*, 1–12.
(13) Nicholson, R. S.; Shain, I. *Anal. Chem.* **1964**, *36*, 706–723.
(14) Saito, Y. *Rev. Polarogr. (Jpn.)* **1968**, *15*, 177–187.
(15) Bonhote, P.; Dias, A. P.; Papageorgiou, N.; Kalyanasundaram, K.; Gratzel, M. *Inorg. Chem.* **1996**, *35*, 1168–1178.
(16) MacFarlane, D. R.; Meakin, P.; Sun, J.; Amini, N.; Forsyth, M. J. *Phys. Chem. B* **1999**, *103*, 4164–4170.
(17) Schröder, U.; Wadhawan, J. D.; Compton, R.; Marken, F.; Suarez, P. A. Z.; Consorti, C. S.; Dupont, R. F. J. *New. J. Chem.* **2000**, *24*, 1009–1015.
(18) Silvester, D. S.; Compton, R. G. *Z. Phys. Chem.* **2006**, *220*, 1247–1274.
(19) Marsh, K. N.; Deev, A.; Wu, A. C. T.; Tran, E.; Klamt, A. *Korean J. Chem. Eng.* **2002**, *19*, 357–362.
(20) Shoup, D.; Szabo, A. J. *Electroanal. Chem. Interfacial Electrochem.* **1982**, *140*, 237–245.
(21) Klymenko, O. V.; Evans, R. G.; Hardacre, C.; Svir, I. B.; Compton, R. G. J. *Electroanal. Chem.* **2004**, *571*, 211–221.
(22) Fietkau, N.; Clegg, A. D.; Evans, R. G.; Villagr′an, C.; Hardacre, C.; Compton, R. G. *ChemPhysChem* **2006**, *7*, 1041–1045.
(23) Montenegro, M. I. *Res. Chem. Kinet.* **1994**, *2*, 9.

JP711897B